Ionospheric influence on the seismo-telluric current related to electromagnetic signals observed before the Wenchuan M_S=8.0 earthquake

Mei Li[1, 2], Handong Tan[2] and Meng Cao[2]

(1) China Earthquake Networks Center, China Earthquake Administration, No.5, Sanlihe Nanhengjie, Xicheng District, 100045 Beijing, China.

(2) China University of Geosciences, No.29, Xueyuan Road, Haidian District, 100083 Beijing, China.

Corresponding author: Handong Tan, China University of Geosciences, No.29, Xueyuan Road, Haidian District, 100083 Beijing, China. (thd@cugb.edu.cn)

Abstract. A three-layer (Earth-air-ionosphere) physical model, as well as a two-layer (Earth-air) model, is employed in this paper to investigate the ionospheric effect on the wave fields for a finite length dipole current source co-located at a hypocenter depth and along the main fault of an earthquake when the distance between the epicenter and an observing station is up to one thousand kilometers or even more. The results show that all electrical fields are free of ionospheric effect for different frequencies in a relative short range, e.g., ～300 km for f=1 Hz, implying the ionospheric influence on electromagnetic fields can be neglected within this range, which becomes smaller as the frequency increases. However, the ionosphere can give a constructive interference to the waves passed through and make them decay slowly when an observation is out of this range and the ionosperic effect can be up to 1-2 magnitudes of the electrical fields. For an ground-based observable 1.3 mV m^{-1} electric signal at f=1 Hz at 1,440 km away from the Wenchuan M_S=8.0 earthquake, the expected seismo-telluric current magnitude for the Earth-air-ionosphere model is of 5.0×10^7 A, one magnitude smaller than the current value of 3.7×10^8 A obtained by the Earth-air model free of ionospheric effect. This indicates that the ionosphere facilitates the electromagnetic wave propagation, as if the detectability of the system is improved effectively and it is easier to record a signal even for stations located at distances beyond their detectability threshold. Furthermore, the radiating patterns of the electrical field components |Ex| and |Ey| are complementary each other although anyone 2-D power distribution of them shows strong power areas as well as weak

ones, which is advantageous to register a signal if the observing system is designed to measure both of them instead of only one.

Keywords. Ionospheric influence on electromagnetic waves; The Wenchuan earthquake; Seismo-telluric current; 2-D power distribution

1 Introduction

The fact that Electro-Magnetic (EM) emissions accompany every stage of large earthquake preparations seems undebatable although short-term earthquake prediction is still one of the most challenging targets in Earth science today (Eftaxias et al., (2002). Meanwhile, the Ultra-Low Frequency (ULF) band is of particular interest because only EM signals in the ULF range and at lower frequencies originated in the Earth's crust can be easily recorded at the Earth's surface without significant attenuation comparing with 'high' frequency emissions that might be emitted at epicenter depths at more than 10 km, even several hundreds of kilometers. Recently, an increasing number of ground-based observing ULF electromagnetic emissions related to strong earthquakes have been recorded at a distance of several, hundred, and even several thousand kilometers. Some notable examples include the Loma Prieta *M*s=7.1 earthquake on October 17, 1989 (f=0.01-10 Hz, D=7 km, A=1.5 nT) (Fraser-Smith et al., 1990; Bernardi et al., 1991), as well as the Spitak M_S=6.9 earthquake on December 7, 1988 (f=0.005-1 Hz, D=200 km, A=0.2 nT) (Molchanov et al., 1992; Kopytenko et al., 1993). In addition, the geo-electric potential enhancement appeared 1–19 days before five of all six EQs with magnitude >5 that occurred within 75 km in Japan and its duration and intensity were several minutes to 1 h with an amplitude of 0.01–0.02 mV m^{-1} (Uyeda et al., 2000). Qian *et al*. (2002) have reported the observation of ULF signals generated from Jiji earthquake of 21 September 1999 in Taiwan and recorded at many stations at distances of 300–900 km in South East China. Similarly, Ohta *et al*. (2002) have reported the observation of ULF/ELF emissions generated from Taiwan earthquake of 21 September, 1999 and recorded at Nakatsugawa station in Japan at a distance of up to 2000 km.

A more notable example reported by Li et al. (2013) is the Wenchuan *M*s=8.0 earthquake on May 12, 2008, a typical mid-crust, which resulted in great devastation and 69,000 deaths. This earthquake was preceded by more than one month of increasing anomalous ULF emissions with a climax starting on May 9, three days

before the Wenchuan main shock (f=0.1-10 Hz, D=1,440 km, A=1.3 mV m-1).

Many simulating rock-pressure experiments were carried out in order to understand the producing mechanism of the electromagnetic information associated with seismic activities. Laboratory experiments by *Qian et al*., [1996; 2003] and *Hao et al*. [2003] present that, electromagnetic signals are always recorded when rock samples are subjected to dynamic stresses. Electromagnetic pulses of shorter-period appearing at the last stage of the experiment may be induced by instantaneous electric current of the accumulated charge during the stress acceleration.The work of Freund et al. (Freund and Wengeler, 1982, Freund, 2002, 2009, 2010; Freund and Sornette, 2007; Scoville et al., 2015) has gained a new insight into the production of current and electromagnetic signals in stressed rocks. As rocks upon stressing, stresses cause slight displacements of mineral grains in the rocks, which in turn lead to the activation of peroxy defects that preferentially sit on or across grain boundaries. The peroxy break-up leads to positive holes h^* and the $h^*$are able to flow from stressed to unstressed rock, traveling fast and far by way of a phonon-assisted electron hopping mechanism using energy levels at the upper edge of the valence band. A gabbro sample（30×15×10 cm^3）from Shanxi, China, was used in the test and a 55 nA current recorded about 2 seconds before failure, with the load being at about 30,000 lbs and the maximum spike reaches 450 nA when the main failure took place (Freund, 2009).

Up to now, no clear explanation has been given although several physical mechanisms have been proposed to interpret the generation of EM emissions and electrical currents observed either during seismic activity or in the laboratory experiments. These include the electrokinetic and magnetohydrodynamic, piezomagnetism, stress-induced variations in crustal conductivity, microfracturing, and so on (Draganov et al., 1991; Park, 1996; Fenoglio et al., 1995; Egbert, 2002; Simpson and Taflove, 2005). Whatever the physical mechanism of electromagnetic generation is, it is well established that, during rock experiments conducted under laboratory conditions, a strong electrical current is produced when rocks are stressed, especially at the stage of the main rupture.

As the development of satellite Earth Observation (EO), there is an increasing amount of evidence that during some last stages of the long term process of preparation, there could be a transfer of energy between lithosphere, atmosphere and ionosphere, so as to introduce the concept of a lithosphere–atmosphere–ionosphere coupling (LAIC) among the three involved layers of the Earth (Pulinets et al., 1994,

2000; Hayakawa and Molchanov, 2002; Molchanov et al., 2004; Kamogawa, 2006). When we investigate electromagnetic emissions induced by an electrical current or a magnetic moment on the surface or beneath the Earth, the effect of the medium air, crustal as well as ionosphere should be taken into account because of these three media being of different conductivities and so we need to consider a lithosphere-atmosphere-ionosphere electromagnetic coupling (Cummer, 2000). Several tentative LAIC models have been constructed based on ground-based and ionospheric observations prior to strong earthquakes and the investigation of influence of external electrical filed on ionospheric parameters has been developed quickly (Pulinets and Ouzounov, 2011; Pulinets and Davidenko, 2014; Sorokin and Hayakawa, 2013; Sorokin and Hayakawa, 2014; Kuo et al., 2011, 2014; Namgaladze et al., 2012; Zolotov et al., 2012; Zolotov, 2015). At the same time, the ionosphere plays an important role in electromagnetic propagation at Extremely Low Frequency (ELF) and Very Low Frequency (VLF), the ground and the ionosphere are good electrical conductors and form a spherical Earth-ionosphere waveguide (Cummer, 2000). In addition, in the Controlled Source Electromagnetic (CSEM) method, widely used in petroleum exploration or mining, the ionospheric influence on electromagnetic (EM) fields should be considered when the distance between a large-scale and large-power fixed source and the receiver is up to one thousand kilometers. EM fields can be amplified in the ionosphere as it is shown when we use analytical solutions of Maxwell equations, as well as numerical ones of the “Earth-ionosphere” mode with a source on the Earth’s surface or in the lower atmosphere (Fu et al., 2012; Li et al., 2010a; Li et al., 2010b; Xu et al., 2012; Li et al., 2011).

Therefore, comparing with an electromagnetic attenuation without ionospheric effect, the point is to evaluate the ionospheric influence on the electromagnetic propagation when the distance between the epicenter and the observing location is up to one thousand kilometers or even more. Furthermore, the comparison between the observation distance reported by Li et al. (2013) (D=1,440 km) and the length of the Wenchuan earthquake main rupture L=～150 km (Zhang et al., 2009) indicates that the length of the dipole source is not negligible. So in this paper, based on the work of Key (2009), a three-layer (Earth-air-ionosphere) physical model, as well as a two-layer (Earth-air) model, containing a finite length dipole current source co-located along the fault and beneath the Earth is introduced in Sect. 2. For specified parameters, some simulation results of the current source with and without

ionospheric effect are given in Sect. 3. In Sect.4, using assumed parameters, the simulation results for the case of the Wenchuan earthquake reported by Li et al. (2013) are presented. Discussion and conclusions are given in Sect. 5 and Sect.6, respectively.

2 Description of the modeling methodology

In order to study the electromagnetic fields emitted by a long dipole current source, the approach used here follows the magnetic vector potential formulation described in Wait (1982) and developed by Key (2009), who generalized the formulation to allow for multiple layers above the transmitter (in addition to multiple layers below). He used exponential forms for the recursions rather than hyperbolic functions in isotropic media, which consists of N layers of isotropic conductivityσ_i where$i = 1, \ldots, N$, and which uses a right-handed coordinate system with the z axis pointing down. Assuming a time-harmonic source with $e^{-i\omega t}$ time dependence, negligible magnetic permeability μ variations, and angular frequencies ω that are low enough so that displacement currents can be neglected, Maxwell's equations are

$$\nabla \times \mathbf{E} = i\omega\mathbf{B}, \qquad (1)$$

and

$$\nabla \times \mathbf{B} = \mu\sigma\mathbf{E} + \mu\mathbf{J}_s\,. \qquad (2)$$

Expression $\mathbf{J}_s = \mathbf{I}\delta(\mathbf{r} - \mathbf{r_0})$ is the imposed electric dipole source at position $\mathbf{r}_0$ with vector moment **I**, and here is restricted to an infinitesimal dipole with unit moment.

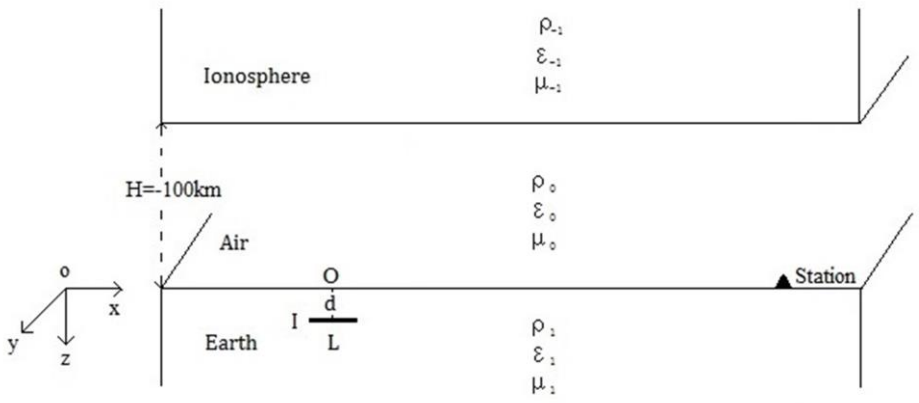

Fig.1. An x-directed dipole current source, with its central coordinate (0, 0, d), is placed in the bottom medium (Earth) of a three layer modeling (Earth-air-ionosphere model), where z is defined positive in the downward direction.

Based on the model set up by Key (2009), some modifications will be done in this study in order to answer the questions illustrated above. A physical model is specified. It has three layers, Earth, air and ionosphere, which is called Earth-air-ionosphere model. Its coordinate system is denoted in Fig.1 with z-direction being downward. An x-directed dipole of a length L and a current I is placed in the bottom medium (Earth: $z > 0$), which is homogeneous and has the electrical properties: magnetic permeability μ_1, permittivity ε_1, and conductivity σ_1. The middle medium (air: $-100\ \text{km} < z < 0$) is described by its electrical properties μ_0, $\varepsilon_0 (= 8.854 \times 10^{-12}\ \text{Farad m}^{-1})$ and $\sigma_0 (= 10^{-14}\ \text{S m}^{-1})$. The top medium (ionosphere: $z < -100\ \text{km}$) is characterized by electrical properties μ_{-1}, ε_{-1} and $\sigma_{-1} (= 10^{-5}\ \text{S m}^{-1})$.

As a comparison, a two-layer model (Earth-air model) including in Earth medium ($z > 0$), as well as air medium ($z < 0$), is also established during the study. All the corresponding parameters described are the same as these of Earth-air-ionosphere model.

We assume that the total space is non-magnetic and that the magnetic permeabilityμvariations are negligible in the different layers, i.e. $\mu_1 = \mu_0 = \mu_{-1} = 4\pi \times 10^{-7}\ \text{Farad m}^{-1}$. However, the ionosphere as the electrically conducting section of the upper atmosphere plays such an important role for the electromagnetic propagation that we set $\varepsilon_{-1} = 5\varepsilon_0$ when an ionospheric effect on electromagnetic transmission is taken into consideration. On the same manner we have $\varepsilon_1 = \varepsilon_0 = 8.854 \times 10^{-12}\ \text{Farad m}^{-1}$, i.e. ε_1 is not considered as zero during all calculations. Under these conditions, the formula listed above are still suitable and more explanations about the potential formulation of a horizontal electric dipole can be found in the Appendix A of Key (2009) and related programs are available with an access to the website (http://marineemlab.ucsd.edu/). The horizontal finite length dipole source can be viewed as integral of an infinite small horizontal dipole during related calculations.

3 Simulation results

According to these two models presented above, several free parameters must be specified in order to investigate the attenuation characteristics of the electromagnetic fields emitted by a long x-directed dipole current source. As for the parameters of the dipole current source, we select L=150 km, the Wenchuan earthquake main rupture

stage within 30 s out of 90 s (～300 km) based on Zhang et al., (2009, Fig.1), the depth d =19 km (Xu, 2009), the hypocenter depth of the Wenchuan case and the current is set to be I=1 A temporarily. Here, the Earth is considered to be an isotropic media with an average conductivity σ_1, and we assume $\sigma_1 = 1.0 \times 10^{-3}$ S m^{-1} at this time, i.e.$\rho_1 = 10^3$ ohm · m, although the ground conductivity depends not only on the local petrology, but also on the porosity, temperature, and pressure (e.g., Wait, 1966). All these parameters are common to two models. The parameter $\varepsilon_{-1} = 5\varepsilon_0$ is of most importance during the calculation in three-layer model in that it can potentially affect the transmission of electromagnetic waves produced by the dipole beneath the Earth, and possibly induce the Earth-atmosphere-ionosphere electromagnetic coupling.

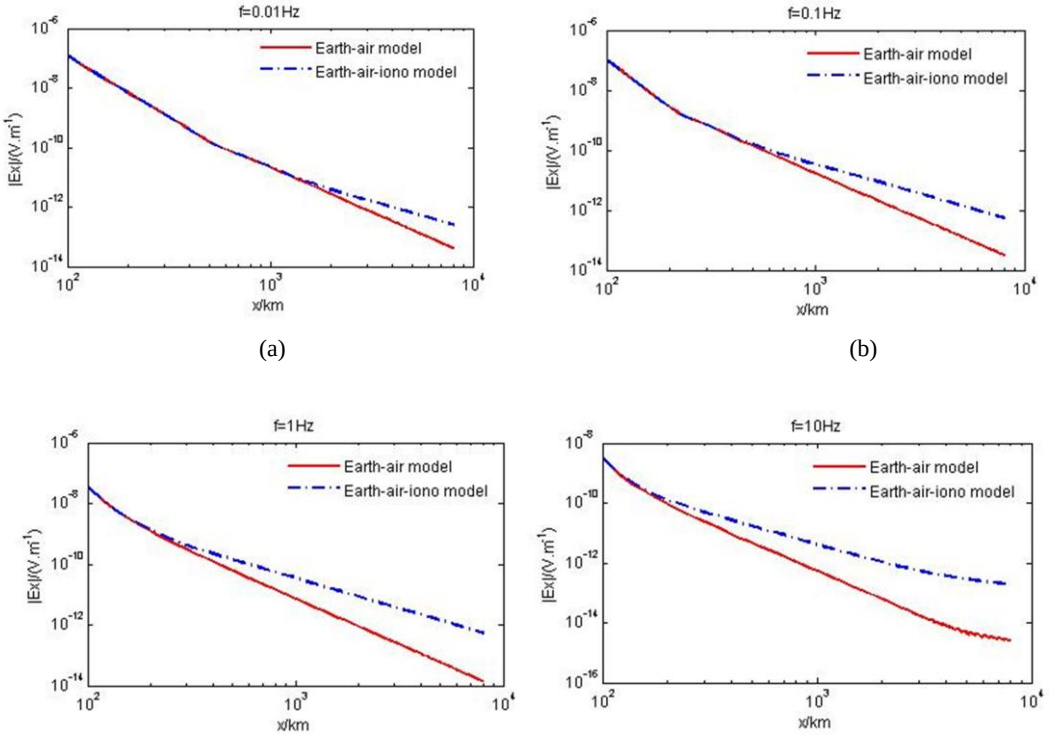

Fig.2. Electric field $|E_x|$ decay curves along x-axial direction as a function of the observing distance for the Cartesian coordinate system with different frequencies. Red solid lines stand for electric field curves for Earth-air model and blue dot lines denote electric field curves with the ionospheric effect for Earth-air-ionosphere model.

(a) Total $|E_x|$ for f=0.01 Hz; (b) Total $|E_x|$ for f=0.1 Hz;

(c) Total $|E_x|$ for f=1 Hz; (d) Total $|E_x|$ for f=10 Hz;

Fig.2a-d displays electric field amplitude $|E_x|$ decay curves along the x-axial direction with the frequencies f=0.01 Hz, f=0.1 Hz, f=1 Hz, and f=10 Hz respectively for the Cartesian coordinate system up to ～10,000 km on the Earth's surface.

It can be seen from Fig.2a-d, first, the electrical field with "high" frequency has a big attenuation although all curves for both Earth-air model (red solid lines) and Earth-air-ionosphere model (blue dot lines) decay rapidly as the distance increases. Second, each group of curves run at the same level for one fixed frequency, e.g., f=1 Hz, when an observing point is located at a relative near distance, ～300 km for f=1 Hz (Fig.2c) for example. That is to say, the ionospheric influence on electromagnetic field transmissions can be neglected within this range. However this range changes for different frequencies and it becomes smaller as the operating frequency of the current source increases (e.g., more than 1000 km for f=0.01 Hz (Fig.2a) and only ~200 km for f=10 Hz (Fig.2d)). Third, the most important result is, as the distance increases, field curves with an ionospheric effect (blue dot lines) run along a different path from that of curves without an ionospheric effect (red solid lines) and the ionospheric lines attenuate more slowly. Now, this kind of ionospheric influence can no longer be neglected. The ionospheric difference is about 1 magnitude (×10) for all the frequencies listed and even once up to 2 magnitudes for f=10 Hz within the range shown in Fig.2. For example, the ionospheric difference value shows 1 magnitude from ～840 km, up to 2 magnitudes from ～3,700 km for f=10 Hz (Fig.2d).

4 The Wenchuan M_S=8.0 earthquake as a sample

4.1 Estimating the seismo-telluric current magnitude

On the base of the work of rock experiments conducted under laboratory conditions, there is a reason to believe that a giant seismo-telluric current is generated when the main rupture took place during the Wenchuan earthquake on 12 May 2008 and that this current mainly propagated along the Longmenshan fault. At the same time a strong electrical field induced by this current suddenly increased. This electrical field was recorded at the ground-based Gaobeidian ULF observing station, 1440 km away from the epicenter of the shock, with a SN (South-North) maximum amplitude of 70 mm, i.e. 1.3 mV m^{-1} (Li et al., 2013), that is $E_{obs(SN)}$ = 1.3 mV m^{-1} in the following statement (Fig. 3).

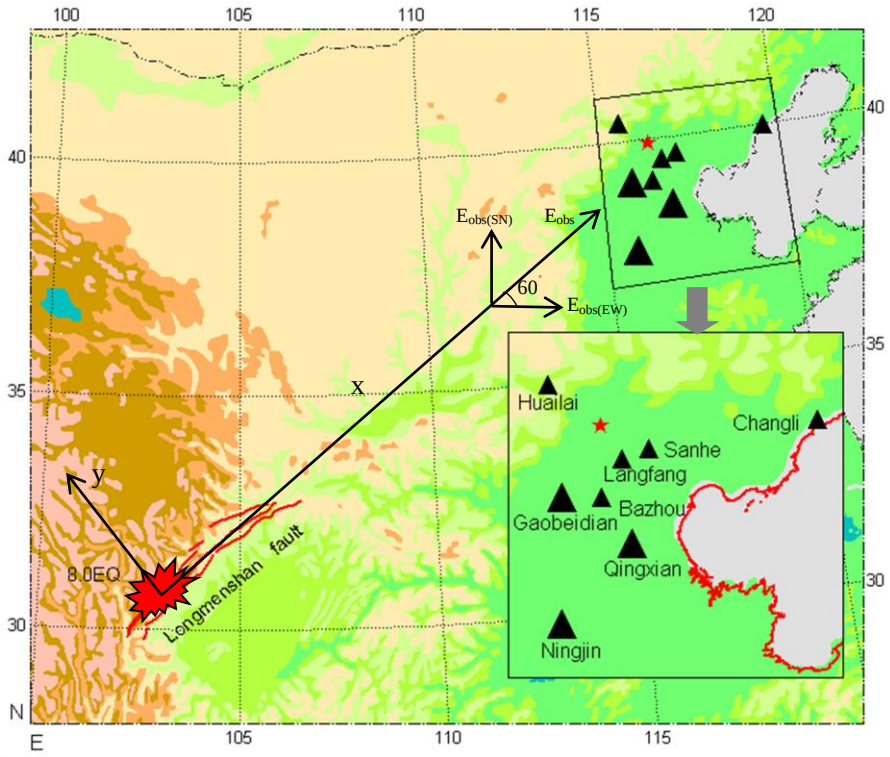

Fig.3. Distribution of the Wenchuan earthquake epicenter and observation stations. Black solid triangles present the related locations of observation stations in Hebei electromagnetic observation network, bigger ones indicate the stations where abnormal information was recorded and the red star denotes Beijing (Li et al., 2013, Fig.1). A ground surface coordinate system is added.

In order to establish a relationship between the seismo-telluric current during the main event and the observable ground electrical signals registered at Gaobeidian station, we consider that a finite length current dipole source, with the length being the main rupture L=150 km of the Wenchuan earthquake and the current I, is co-located with the Longmenshan main fault (x-direction), with the depth being d=19 km. Then one can refer to Fig.1 with ionospheric effect.

Corresponding to Fig.1, a coordinate system on the Earth's surface (see Fig.3) is set up to calculate the observable electrical field along the x-direction E_{obs} according to the electrical value $E_{obs(SN)}$=1.3 mV m^{-1} recorded at the Gaobeidian station. The Gaobeidian station lies in the extended line of the Longmenshan fault, which trends northeast and dips about 60 °west (Xu, 2009). Other locations of stations are shown in Fig.1 of Li et al. (2013) and here they are shown in Fig.3 which includes a ground surface coordinate system. From Fig.3, we see that the electrical filed component

intensity along the x-direction is about $|E_x|$=E_{obs}=1.5 mV m^{-1} ($E_{obs(SN)}$=sin60 °× E_{obs}=1.3 mV m^{-1} → E_{obs}=1.5 mV m^{-1}).

As the observing frequency of the electromagnetic observation system is 0.1-10 Hz and the recorder belongs to a real-time analog record, it is not easy to figure out the right frequency of the signals registered at the Gaobeidian station during the maximum stage prior to the Wenchuan earthquake. We set the main frequency f=1 Hz during our calculations although the information is of a short period ~0.1-0.3 s and a large amplitude ~1.3 mV m^{-1} (Li et al., 2013) and frequency bands (0.4-3 s and 0.05-0.1 s) with various amplitudes were observed (Guan et al., 2003). At the same time, the results of 2D MT inversion in the Longmenshan fault show that the apparent resistivity logarithm is ～1-4.8 (Zhu et al., 2008) and it is a wide range.

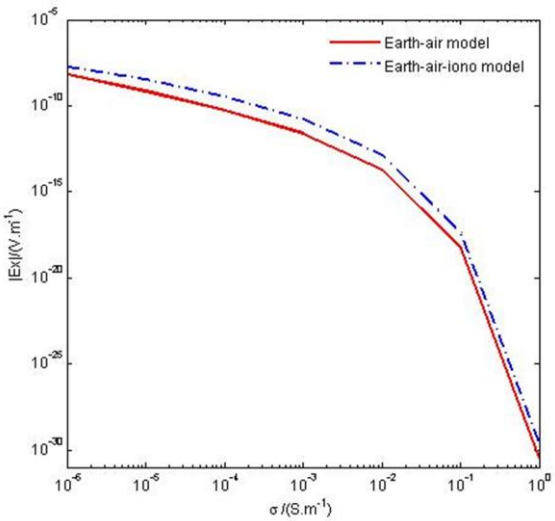

Fig.4. The calculated value of |Ex|, expected at the observation location (1,440 km, 0, 0) due to a dipole source of L=150 km, I=1 A, f=1 Hz and d=19 km (Fig.1), as a function of the typical crustal materials conductivity σ both in Earth-air model (red line) and in Earth-air-ionosphere model (blue dot line).

Fig. 4 shows the calculated values of |Ex|, expected at the observation location (1,440 km, 0, 0) due to a dipole source of L=150 km, I=1 A and d=19 km (Fig.1), as a function of the typical crustal materials conductivity σ. Comparing with the red line with the blue dot one, the ionospheric effect is clearly displayed throughout the variation of the crustal conductivity. A rapid attenuation (in excess of 20 of magnitude)

of the field values indicates the importance of the conductivity σ. It is difficult to specify the average conductivity σ (referred to as σ_1 in the context) of the homogeneous Earth medium, even for the typical Wenchuan area. However, combined with f=1 Hz here, the skin-depth depends on the conductivity σ, given by the formula $\delta = (\pi f \mu_0 \sigma)^{-\frac{1}{2}}$. Taken the depth d=19 km into account, here $\delta = d = 19$ km and the calculated σ_1 is attained, i.e. $\sigma_1 = 7.0 \times 10^{-4}$ S m^{-1}, which is advantageous to radiate electromagnetic waves within this depth.

Using the same parameters as above, the simulation results show that the seismo-telluric current along the main fault needed to produce an electrical ground signal $E_{obs(SN)}$ = 1.3 mV m^{-1} at the Gaobeidian station when the Wenchuan event occurred, is about 5.0×10^7 A with the ionospheric effect and 3.7×10^8 A without the ionospheric effect. As it is expected, these two results have one magnitude (×10) difference from each other. While the former is more reasonable under this conditions because the seismo-telluric current produced by the Wenchuan main rupture is specified.

4.2. Detectability under the ionospheric effect

Now according to the Wenchuan earthquake example, the seismo-telluric current source (f=1 Hz, d =19 km, L=150 km, and a current $I=5.0\times10^7$ A considering the Earth-air-ionosphere model) is thought of as a powerful finite length dipole source.

Fig.5 displays the fluctuations of the surface electrical fields with and without ionospheric effect for the Wenchuan source along x-axial direction. It shows no obvious ionospheric effect within 300 km, while this effect is roughly up to 1 order of magnitude from ~800 km. The gap becomes larger as the distance increases, 2 magnitudes from ~4000 km, and then it keeps this gap till 10,000 km. Under this condition, considering the observable signal 1.5 mV m^{-1} at Gaobeidian station before the Wenchuan epicenter, the distance recorded such a signal must be ~1500 km (blue arrow) with ionospheric effect, or it is only ~800 km (red arrow) without ionospheric effect. So the ionosphere facilitates the electromagnetic wave propagation, as if the detectability of the system were improved effectively and it would be easier to record a signal even at stations located beyond their detectability threshold.

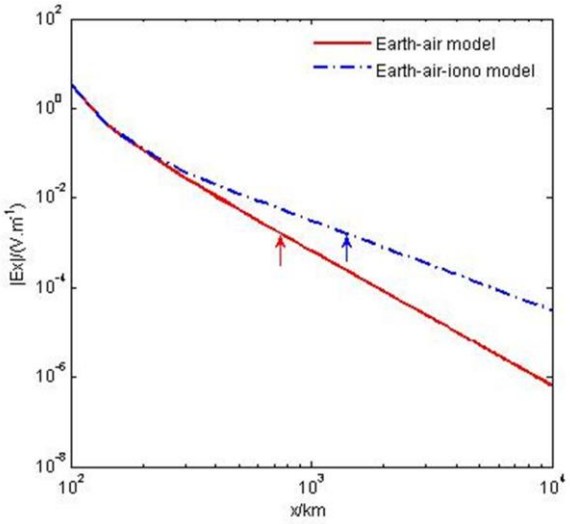

Fig.5. The Wenchuan source producing electric field |Ex| decay curves as a function of the distance along x-axial direction with ionospheric effect (blue dot line), as well as without ionospheric effect (red line). The electric field |Ex|=1.5 mV m^{-1} is labeled by a red arrow and a blue one respectively.

4.3. Wave 2-D distribution

We perform electromagnetic wave fields for the Wenchuan source and this is done in the ground plane region -1,000 km<x<1,000 km and -1,000 km<y<1,000 km in order to visualize the 2-D distribution of the wave power surrounding the electrical source.

Figure 6 displays the 2-D power distributions of the electrical field components |Ex|, |Ey| and the total |E| ($|E|^2=|Ex|^2+|Ey|^2$) after making a logarithm calculation on the Earth's surface. It can be seen firstly from Figure 6a that there is an obvious constant strong power along the current element length (-75 km<x<75 km) in the x-direction. The electrical value in this area is not discussed here because it is usually considered not precise. Then the strong field radiates outward surrounding four main axes, indicating 1 order rough decay of the field at ～160 km, 2 orders of magnitude at ～320 km from the source endpoint in the x-direction. There is only 3 orders decay till 1,000 km away because of the ionospheric facilitating effect on the field and it keeps a strong value (～1.86 mV) which can be fairly recorded by the stations. However, there are also weak power areas along lines, which form 45 °angle with the principal axis for the electrical field power |Ex| (Figure 6a). Complementally, the

electrical field power |Ey| (Figure 6b) is basically characterized by strong power areas between two main axes, as well as weak ones along four chief axes. The power distribution of the total |E| consequently presents to be symmetry to the center circle outside of the source (Figure 6c), which also indicates that the radiating patterns of the electrical field power |Ex| and the electrical field power |Ey| are complementary (One is strong area and the other is weak area) each other surrounding the source.

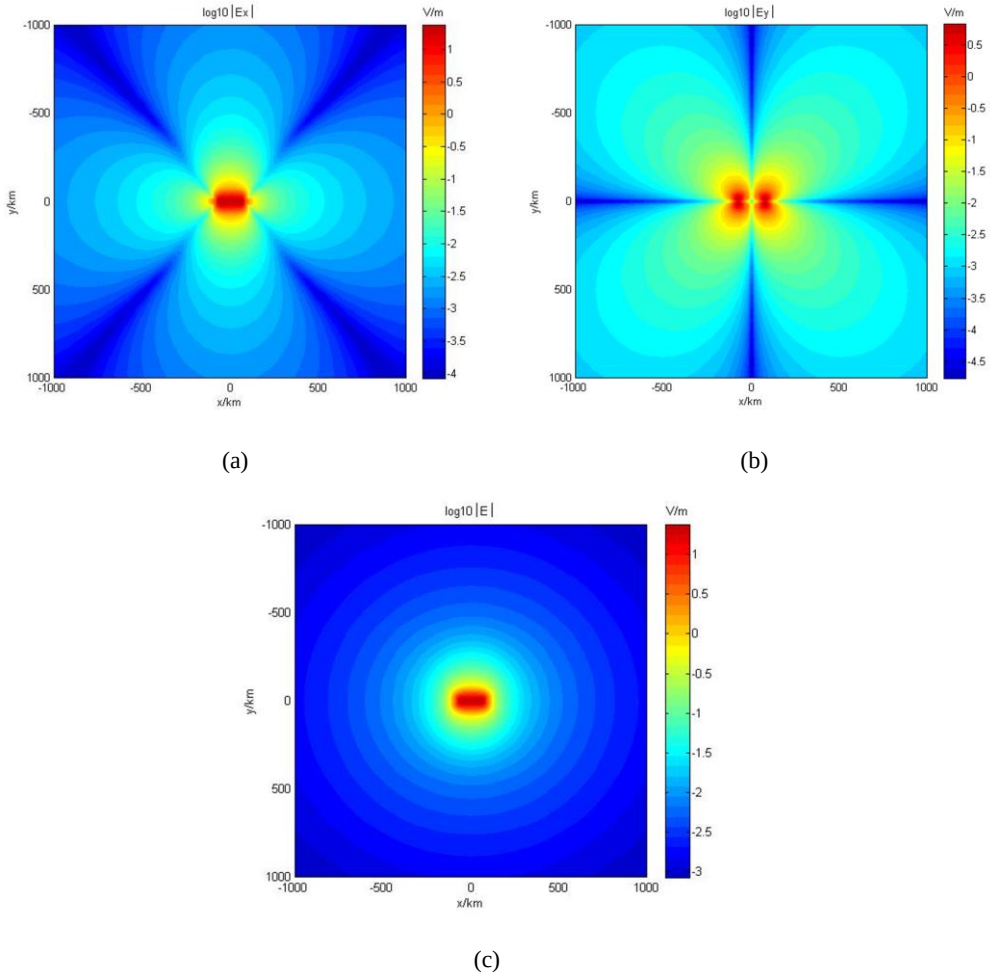

Fig.6. 2-D distributions of electrical field power |Ex| (a), |Ey| (b) and total |E| (c) after a logarithm calculation for the Wenchuan source using Earth-air-ionosphere model.

5 Discussion

In very recent years, there is an increasing amount of evidence that during some last stages of the long term process of preparation, there could be a transfer of energy between lithosphere and the above layers of atmosphere and ionosphere, so as to introduce the concept of a lithosphere–atmosphere–ionosphere coupling (LAIC) among the three involved layers of the Earth system (Pulinets et al., 2000; Hayakawa

and Molchanov, 2002; Molchanov et al., 2004; Pulinets and Ouzounov, 2011). On one hand, the 'energy source' is usually thought to be beneath the Earth's surface and related to tectonic activities in the lithosphere. On the other hand, numerous rock-pressure experiments and electromagnetic observations associated with seismic activities have already proved that a giant electrical current and an abrupt increase of electromagnetic signals occur during the main rupture of stressed-rocks. These phenomena happed on May 9 2008, 3 days before the Wenchuan event, which hypocenter lies in mid-crust. The strong seismo-telluric current is thought to run mainly along the Longmenshan fault and electromagnetic oscillations, induced by the current and predominated by ULF frequency band, propagate up to ionosphere and give rise to perturbations of ionospheric parameters. Some of these parameters have been investigated, such as GPS TEC and f0F2 (Yu et al.， 2009; Xu et al., 2010; Akhoondzadeh et al., 2010), DEMETER satellite O+ density (Zhang et al., 2009), electron density and electron temperature (Zeng et al., 2009), and so on. Fortunately, all these study results present a climax on May 9 and this indicates a lithosphere–atmosphere–ionosphere coupling or interaction aroused by these electromagnetic signals prior to the Wenchuan event.

Unfortunately, at present, most of investigations put emphases on the effect of earthquakes upon the ionosphere and few of them pay attention to an inverse problem, that is the ionospheric influence on the electromagnetic waves passing through.

The ionosphere, as a part of the electrical conducting region of the upper atmosphere, can enhance electromagnetic fields and cause the decay as a function of distance to slow down when an observation is within ionospheric range and the ionosperic effect can be up to 1-2 magnitudes of the electrical fields in our simply three-layer model for some specified parameters we have selected here.

Considering the Wenchuan event, the electrical signals from the lithosphere interact with the ionosphere and are at the same time enhanced, and then registered at 1440 km Gaobeidian station with the amplitude of 1.3 mV m^{-1}. This electrical field is used to simulate the seismo-telluric current produced by the Wenchuan main rupture in an Earth-air-ionosphere model together with an Earth-air model. The results present that, the seismo-telluric currents with and without ionospheric effect must be about 5.0×10^{7} A and 3.7×10^{8} A respectively. Compared with the expected seismo-telluric current ~10–100 kA of the "Alum Rock" M_W=5.6 earthquake for an observed 30 nT pulse at 1 Hz and D=2 km (Bortnik et al., 2010), this result is probably in a reasonable

481 range.

482 However, firstly, the total rupture of the Longmenshan fault during the
483 Wenchuan main shock is extremely complicated that comprises of tenths of rupture
484 stages and several pauses, totaling 90 s for the whole rupture process (～300 km),
485 according to Zhang et al.,(2009). Thus the total surface rupture ～300 km is
486 nevertheless not used here. While performing the analysis on only the primary 30 s, a
487 main stage of the Wenchuan earthquake, out of 90 s as we have selected L=150 km
488 above, is expected to be representative of the majority of the rupture to generate a
489 seismo-telluric current. Secondly, three medium are thought of as a homogeneous
490 isotropic medium in our models and with the same average conductivity value for
491 each one, especially for the wenchuan area. However, the Earth conductivity plays
492 such an important role that it predominately affects the fluctuations of the electrical
493 fields as shown in Fig.4 although no one exactly knows the right conductivity of the
494 Earth medium at the rupture depth. The value $\sigma_1 = 7.0 \times 10^{-4}$ S m^{-1} taken part in
495 all analysis is estimated when the observing frequency range f=0.1-10 Hz and the
496 hypocenter depth d=19 km of the Wenchuan main event are taken into account for the
497 skin-depth formula. One must also mention that we use f=1 Hz in our calculations
498 because we cannot identify the actual frequencies in the recorded analog signals. All
499 these can probably underscore our simulation results.

500 While these disadvantageous selections maybe are not so important at the same
501 time because the key point of this paper is of the ionospheric influence on
502 electromagnetic wave propagation and our investigation attains advantageous results.

503 The “selectivity” or “orientation” of the electromagnetic information is a very
504 important character during seismic activities (Varotsos and Lazaridou, 1991). For a
505 finite length dipole source of the Wenchuan earthquake, its 2-D distributions of
506 electrical field component |Ex| and |Ey| , which are orthogonal each other, on the
507 Earth’s surface shows there are strong field power areas and weak field power areas
508 around the source as illustrated by [Bortnik et al., 2010]. While the radiating pattern
509 of the total |E| in this investigation is symmetry to the center circle outside of the
510 source which indicates a signal is always registered to anyone direction if a system is
511 designed to measure the total field |E| or both of |Ex| and |Ey| components instead of
512 only one. This result also basically supports the practices of “selectivity” or
513 “orientation”, the observing reality before the Wenchuan earthquake described by Li
514 et al.[2013], for example, ‘Compared with the EW (East-West) orientation, the

electromagnetic signal is more obvious in the SN (South-North) orientation'. The selectivity effect is a complex phenomenon that may be attributed to a superposition of the following three factors: "source characteristics", "travel path" and "inhomogeneities close to the station" [Varotsos and Lazaridou, 1991; Varotsos et al., 2005]. Analytical solutions of Maxwell equations [Varotsos et al., 2000], as well as numerical ones [Sarlis et al., 1999], convince that selectivity results from the fact that earthquakes occur by slip on faults which are appreciably more conductive than the surrounding medium.

6 Conclusions

In this paper, a three-layer (Earth-air-ionosphere) physical model, as well as a two-layer (Earth-air) model, is employed to investigate the ionospheric effect on the wave fields for a finite length dipole current source co-located with the main fault of an earthquake when an observing location distance is up to one thousand kilometers or even more. For a dipole source with specified parameters of the length L=150 km, the current I=1 A, and the depth d=19 km, the results show that all fields are free of the ionospheric effect for different frequencies in relative short ranges, e.g., ～600 km for f=0.1 Hz, which implies the ionospheric influence on electromagnetic field transmissions can be neglected within this range. However, the ionosphere can increase the field amplitude and slow the decay when an observation is out of this range and the ionosperic effect can be up to 1-2 magnitudes of the electrical fields.

This is applicable to the 12 May 2008 Wenchuan M_S=8.0 earthquake during which a strong electromagnetic signal with an amplitude of ~1.3 mV m^{-1}, is recorded by the Gaobeidian ULF (f=0.1-10 Hz) observing station 1440 km from the epicenter. The main fault rupture producing a current is equivalent to a finite length dipole current source, with a nucleation depth of 19 km and a length of 150 km. Considering the Earth-air-ionosphere model, the expected current for the most typical properties of Wenchuan area is of 5.0×10^7 A, which is of one magnitude smaller than the current value of 3.7×10^8 A obtained with the Earth-air model free of ionospheric effect. On the contrary, a signal produced by a seismic activity can be advantageously recorded by a remote station under the ionospheric effect as if the detectability of the system is improved effectively.

The 2-D power distributions of the electrical field component |Ex|, |Ey| and the total |E| after making a logarithm calculation on the Earth's surface are characterized

by different radiating patterns. There are strong power areas along four main axes as well as weak power areas between two main axes for the electrical field |Ex|. While the component |Ey| displays a complementary radiating pattern with strong areas and weak areas. Therefore, fortunately, a signal is always registered to anyone direction if a system is designed to measure the total field |E| (or both |Ex| and |Ey| components) as the radiating pattern of which is Symmetry to the center circle outside of the source.

Acknowledgements and data. The authors are grateful to the National Natural Science Foundation of China and this work was sponsored by the project Simulation and Interpretation of the Spatial Electromagnetic Phenomena Coupling before the Wenchuan M_S8.0 Earthquake under grant agreement n °41204057. The data presented in this paper are available to the e-mail: limeixuxl@seis.ac.cn.

Edited by: C. Krawczyk

Reviewed by: F. Freund and one anonymous reviewer

References

Akhoondzadeh, M., Parrot, M., and Saradjian M. R.: Electron and ion density variations before strong earthquakes (*M*>6.0) using DEMETER and GPS data, Nat. Hazards Earth Syst. Sci., 10, 7–18, 2010.

Bernardi, A., Fraser-Smith, A. C., McGill, P. R., and Villard Jr, O. G.: Magnetic field measurements near the epicenter of the *M*s7.1 Loma Prieta earthquake, Phys. Earth Planet, Interiors, 68, 45–63, 1991.

Bortnik, J., Bleier, T. E., Dunson, C., and Freund, F., Estimating the seismo-telluric current required for observable electromagnetic ground signals, Ann. Geophys., 28, 1615–1624, doi:10.5194/angeo-28-1615-2010, 2010.

Cummer, S.A.: Modeling Electromagnetic Propagation in the Earth-Ionosphere Waveguide, IEEE Transactions on Antennas and Propagation, 48(9), 2–12, 2000.

Draganov, A. B., Inan, U. S., and Taranenko, Y. N.: ULF magnetic signatures at the Earth due to groundwater flow: a possible precursor to earthquakes, Geophys. Res. Lett., 18, 1127–1130, 1991.

Eftaxias, K., Kapiris, P., Polygiannakis, J., Peratzakis, A., Kopanas, J., Antonopoulos, G., and Rigas D.: Experience of short-term earthquake precursors with VLF-VHF electromagnetic emissions, Nat. Hazards Earth Syst. Sci., 3, 217–228, 2002.

Egbert, G. D.: On the generation of ULF magnetic variations by conductivity

fluctuations in a fault zone, Pure Appl. Geophys., 159, 1205–1227, 2002.
Fenoglio, M. A., Johnston, M. J. S., and Byerlee J. D.: Magnetic and electric fields associated with changes in high pore pressure in fault zones: application to the Loma Prieta ULF emissions, J. Geophys. Res., 100 (12), 951–958, 1995.
Fraser-Smith, A. C., Bernardi, A., McGill, P. R., Ladd, M. E., Helliwell, R. A., and Villard Jr, O. G.: Low-frequency magnetic measurements near the epicenter of the *M*s 7.1 Loma Prieta earthquake, Geophys. Res. Lett., 17, 1465–1468, 1990.
Freund, F., and Sornette, D.: Electro-magnetic earthquake bursts and critical rupture of peroxy bond networks in rocks, Tectonophysics, 431, 33–47, 2007.
Freund, F., and Wengeler, H.: The infrared spectrum of OH^- compensated defect sites in C-doped MgO and CaO single crystals. J. Phys. Chem. Solids 43, 129–145, 1982.
Freund, F.: Charge generation and propagation in igneous rocks, J. Geodynamics, 33, 543–570, 2002.
Freund, F.: Conversion of dissolved “water” into molecular hydrogen and peroxy linkages. J. Non-Cryst. Solids 71, 195–202, 1985.
Freund, F.: Stress-activated positive hole charge carriers in rocks and the generation of pre-earthquake signals, in: Electromagnetic Phenomena Associated with Earthquakes, edited by: Hayakawa, M., Transworld Research Network, Trivandrum, India, Chapter 3, 41–96, 2009.
Freund, F.: Toward a unified solid state theory for pre-earthquake signals, Acta Geophys., 58(5), 719–766, 2010.
Fu, C. M., Di, Q. Y., Xu, C., and Wang, M. Y.: Electromagnetic fields for different type sources with effect of the ionosphere, Chinese J. Geophys., 55(12), 3958–3968, doi: 10. 6038/ j. issn. 0001-5733. 2012. 12. 008, 2012(in Chinese with English abstract).
Guan, H. P., Han, F.Y., Xiao, W. J., and Chen, Z.Y.: ULF electromagnetic observation and data processing methods, Earthquake, 23(2), 5–93, 2003(in Chinese with English abstract).
Hayakawa, M., and Molchanov, O. A. (Eds.): Seismo-Electromagnetics: Lithosphere-Atmosphere-Ionosphere Coupling, Tokyo, Japan: TERRAPUB, 2002.
Kamogawa, M.: Pre-seismic lithosphere–atmosphere–ionosphere coupling. Eos 87(40), 2006.
Key, K.: 1D inversion of multicomponent, multi-frequency marine CSEM data: Methodology and synthetic studies for resolving thin resistive layers, Geophysics, 74(2), F9–F20, 2009.
Kopytenko, Y. A., Matiashvili, T. G., Voronov, P. M., Kopytenko, E. A., and Molchanov, O. A.: Detection of ultra-low frequency emissions connected with the Spitak earthquake and its aftershock activity, based on geomagnetic pulsations data

624 at Dusheti and Vardzia observatories, Phys. Earth Planet. Interiors, 77, 85–95,
625 1993.
626 Kuo, C. L., Huba, J. D., Joyce, G., and Lee, L. C.: Ionosphere plasma bubbles and
627 density variations induced by pre-earthquake rock currents and associated surface
628 charges. J. Geophys. Res., 116, A10317, 2011.
629 Kuo, C. L., Lee, L. C., and Huba, J. D.: An improved coupling model for the
630 lithosphere-atmosphere-ionosphere system, J. Geophys. Res. Space Physics, 119(4),
631 3189–3205, 2014.
632 Li, M., Lu, J., Parrot, M., Tan, H., and Zhang, X.: Review of unprecedented ULF
633 electromagnetic anomalous emissions possibly related to the Wenchuan M_S = 8.0
634 earthquake，on 12 May 2008． Nat． Hazards Earth Syst． Sci．, 13(2), 279–286,
635 doi: 10. 5194/nhess-13-279-2013, 2013.
636 Li, D., Di, Q. Y., and Wang, M. Y.: One-dimensional electromagnetic fields forward
637 modeling for “earth–ionosphere” mode. Chinese J. Geophys., 54(9), 2375–2388,
638 doi: 10. 3969/ j. issn. 0001–5733. 2011. 09. 021, 2011 (in Chinese with English
639 abstract).
640 Li, Y., Lin, P. R., Zheng, C. J., Shi, F. S., Xu, B. L., and Guo, P.: The electromagnetic
641 response modeling of the ELF method and the influence of the ionosphere,
642 Geophysical & Geochemical Exploration, 34(3), 332–339, 2010a, (in Chinese with
643 English abstract).
644 Li, D. Q., Di, Q. Y., and Wang, M. Y.: Study of large scale large power control source
645 electromagnetic with “Earth–ionosphere” mode, Chinese J. Geophys., 53(2), 411–
646 420, doi: 10. 3969/ j. issn. 0001-5733. 2010. 02. 019, 2010b, (in Chinese with
647 English abstract).
648 Molchanov, O. A., Kopytenko, Y. A., Voronov, P. M., Kopytenko, E. A., Matiashvili, T.
649 G., Fraser-Smith, A. C., and Bernardi, A.: Results of ULF Magnetic field
650 measurements near the epicenters of the Spitak (*M*s 6.9) and Loma Prieta (*M*s7.1)
651 earthquakes: comparative analysis, Geophys. Res. Lett., 19, 1495–1498, 1992.
652 Molchanov, O. A., Fedorov, E., Schekotov, A., Gordeev, E. , Chebrov , V., Surkov,
653 V., …, Biagi, P. F.: Lithosphere-atmosphere-ionosphere coupling as governing
654 mechanism for preseismic short-term events in atmosphere and ionosphere, Natural
655 Hazards Earth Syst. Sci., 4, 757-767, 2004.
656 Namgaladze, A. A., Zolotov, O. V., Karpov, M. I., and Romanovskaya,Y.V.:
657 Manifestations of the earthquake preparations in the ionosphere total electron
658 content variations. Natural Science, 4(11), 848–855, 2012.
659 Ohta, K., Umeda, K., Watanabe, M. and Hayakawa, M.: Relationship between ELF
660 magnetic field and Taiwan earthquake. In Lithosphere-Atmosphere-Ionosphere
661 Coupling (eds M. Hayakawa and O. A. Molchanov), Terra Science Publishers,
662 Tokyo, pp. 233–237, 2002.

663 Panfilov, A. A.: The results of experimental studies of VLF–ULF electromagnetic
664 emission by rock samples due to mechanical action, Nat. Hazards Earth Syst. Sci.,
665 14, 1383–1389, doi:10.5194/nhess-14-1383-2014, 2014.
666 Park, S. K.: Precursors to earthquakes: seismo-electromagnetic signals, Surv.
667 Geophys., 17, 493–516,1996.
668 Pulinets, S. A., and Davidenko, D.: Ionospheric precursors of earthquakes and Global
669 Electric Circuit. Advances in Space Research, 53(5), 709–723, 2014.
670 Pulinets, S. A., and Ouzounov, D.: Lithosphere-Atmosphere-Ionosphere Coupling
671 (LAIC) model-An unified concept for earthquake precursors validation, J.
672 Southeast Asian Earth Sci., 41(4–5): 371–382, 2011.
673 Pulinets, S. A., Boyarchuk, K. A., Hegai, V. V., Kim, V. P., and Lomonosov, A. M.:
674 Quasielectrostatical model of atmosphere-thermosphere-ionosphere coupling, Adv.
675 Space Res., 26, 1209-1218, 2000.
676 Pulinets, S.A., Legen'ka, A.D., Alekseev, V.A., 1994. Pre-earthquakes effects and
677 their possible mechanisms. In: Dusty and Dirty Plasmas, Noise and Chaos in Space
678 and in the Laboratory. Plenum Publishing, New York, pp. 545–557.
679 Qian, S., Hao, J., Zhou, J. and Gao, J.: Precursory Electric and Magnetic Signals at
680 ULF and LF Bands during the Fracture of Rocks under Pressure. Earthquake
681 Research in China, 19(2), 109–116, 2003 (in Chinese with English abstract).
682 Qian, S., Hao, J., Zhou, J. and Gao, J.: Simulating experimental study on ULF
683 electromagnetic precursors before Jiji *M*s = 7.4 earthquake. In
684 Lithosphere-Atmosphere-Ionosphere Coupling (eds Hayakawa, M. and Molchanov,
685 O. A.), Terra Science Publishers, Tokyo, pp. 49–53, 2002.
686 Qian, S., Ren K., Lü, Z.: Experimental study on VLF, MF, HF and VHF
687 electromagnetic radiation characteristics with the rock breaking, Earthquake
688 Science, 18(3), 346–351, 1996 (in Chinese with English abstract).
689 Sarlis, N., Lazaridou, M., Kapiris, P., and Varotsos, P.: Numerical model of the
690 selectivity effect and the V/L criterion, Geophys. Res. Lett., 26, 3245–3248, 1999.
691 Scoville, J., J. Sornette, and Freund, F. T.: "Paradox of peroxy defects and positive
692 holes in rocks Part II: Outflow of electric currents from stressed rocks." Journal of
693 Asian Earth Sciences 114, Part 2: 338-351, 2015.
694 Simpson, J. J., and Taflove, A.: Electrokinetic effect of the Loma Prieta earthquake
695 calculated by an entire-Earth FDTD solution of Maxwell's equations. Geophys. Res.
696 Lett., 32, L09302, doi: 10. 1029/2005GL022601, 2005.
697 Sorokin, V. M., and Hayakawa, M.: Generation of Seismic-Related DC Electric
698 Fields and Lithosphere-Atmosphere-Ionosphere Coupling. Modern Applied
699 Science, 7(6), 1–25, 2013.
700 Sorokin, V. M., and Hayakawa, M.: Plasma and Electromagnetic Effects Caused by
701 the Seismic-Related Disturbances of Electric Current in the Global Circuit. Modern
702 Applied Science, 8(4), 61–83, 2014.

703 Uyeda, S., Nagao, T., Orihara, Y., Yamaguchi, T., and Takahashi I.: Geoelectric
704 potential changes: Possible precursors to earthquakes in Japan, Proc. Nat. Acad.
705 Sci., 97, 4561–4566, 2000.
706 Varotsos, P., and Lazaridou, M.: Latest aspects of earthquake prediction in Greece
707 based on seismic electric signals. Tectonophysics, 188, 321–347,1991.
708 Varotsos, P., Sarlis, N., and Lazaridou, M.: Transmission of stress induced electric
709 signals in dielectric media, Part II, Acta Geophys, 48, 141–177, 2000.
710 Varotsos, P., Sarlis, N., Skordas, E., Tanaka, H., and Lazaridou, M.: Additional
711 evidence on some relationship between seismic electric signals and earthquake
712 source parameters, Acta Geophys., 53, 293–298, 2005.
713 Wait, J. R.: Geo-electromagnetism: Academic Press,1982.
714 Wait, J. R.: Some Factors Concerning Electromagnetic Wave Propagation in the
715 Earth's Crust, Proc. IEEE, 54(8), August 1966.
716 Xu, C., Di, Q. Y., Fu, C. M. and Wang, M. Y.: The contrast of response
717 characteristics between large power long dipole and circle source, Chinese J.
718 Geophys, 55(6), 2097–2104, doi: 10. 6038/ j. issn. 0001–5733. 2012. 06. 03, 2012,
719 (in Chinese with English abstract).
720 Xu, T., Hu, Y., Wu, J., Wu, Z., Suo, Y., and Feng, J.: Giant disturbance in the
721 ionospheric F2 region prior to the *M*8.0 Wenchuan earthquake on 12 May 2008,
722 Ann. Geophys., 28, 1533–1538, 2010.
723 Xu, X. W.:Album of 5.12 Wenchuan 8.0 earthquake surface ruptures. Seismological
724 press, 2009 (in Chinese with English abstract).
725 Yamauchi, T., Maekawa, S., Horie, T., Hayakawa, M., and Soloviev, O.:
726 Subionospheric VLF/LF monitoring of ionospheric perturbations for the 2004
727 Mid-Niigata earthquake and their structure and dynamics, J. Atmos. Sol. Terr.
728 Phys., 69, 793–802, 2007.
729 Yu, T., Mao, T., Wang, Y. G., and Wang, J. S.: Study of the ionospheric anomaly
730 before the Wenchuan earthquake, Chinese Science Bulletin, 54(6): 1086–1092, doi:
731 10.1007/s11434-008-0587-8, 2009 (in Chinese with English abstract).
732 Zeng, Z. C., Zhang, B., Fang, G. Y., Wang, D. F., and Yin, H. J.: The analysis of
733 ionospheric variations before Wenchuan earthquake with DEMETER data, Chinese
734 J. Geophys., 52(1): 11–19, 2009 (in Chinese with English abstract).
735 Zhang, X., Shen, X., Liu, J., Ouyang, X., Qian, J., and Zhao, S.: Analysis of
736 ionospheric plasma perturbations before Wenchuan earthquake. Nat. Hazards Earth
737 Syst. Sci., 9: 1259–1266, 2009.
738 Zhang ,Y., Feng, W. P., Xu, L. S., Zhou, C. H., and Chen, Y. T.: Spatio-temporal
739 rupture process of the 2008 great Wenchuan earthquake, Science in China Series D:
740 Earth Sciences, 52 (2), 145–154, 2009.

741 Zhu, Y. T., Wang, X. B., Yu, N., Gao, S. Q., Li, K., and Shi, Y. J.: Longmenshan
742 magnetotelluric deep structure and the Wenchuan earthquake (M_S8.0), Acta
743 Geologica Sinica, 82 (12), 1769–777, 2008 (in Chinese with English abstract).
744 Zolotov, O. V.: Ionosphere Quasistatic Electric Fields Disturbances over Seismically
745 Active Regions as Inferred from Satellite_Based Observations: A Review. Russian
746 Journal of Physical Chemistry B, 9(5), 85–788, 2015.
747 Zolotov, O. V., Namgaladze, A. A., Zakharenkova, I. E., Martynenko, O. V.,
748 andShagimuratov, I. I.: Physical Interpretation and Mathematical Simulation of
749 Ionospheric Precursors of Earthquakes at Midlatitudes. Geomagnetism &
750 Aeronomy, 52(3), 390–397, 2012.
751
752